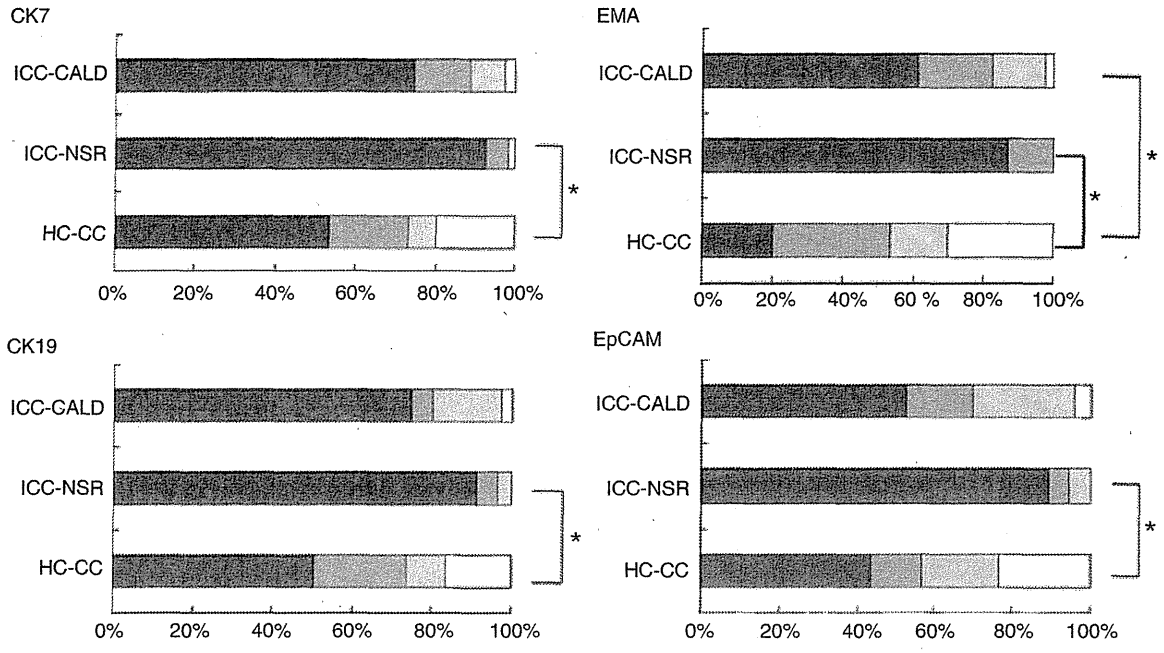

Figure 3. Expression of cytokeratin (CK)7, CK19, epithelial membrane antigen (EMA) and epithelial cell adhesion molecule (EpCAM) in intrahepatic cholangiocarcinoma (ICC) with chronic advanced liver disease (CALD), ICC with non-specific reactive changes (NSRs), and combined hepatocellular cholangiocarcinoma (HC-CC). □, negative (0%); ▫, 1–10%; ▩, 11–50%; and ■, >50%; *$P < 0.05$.

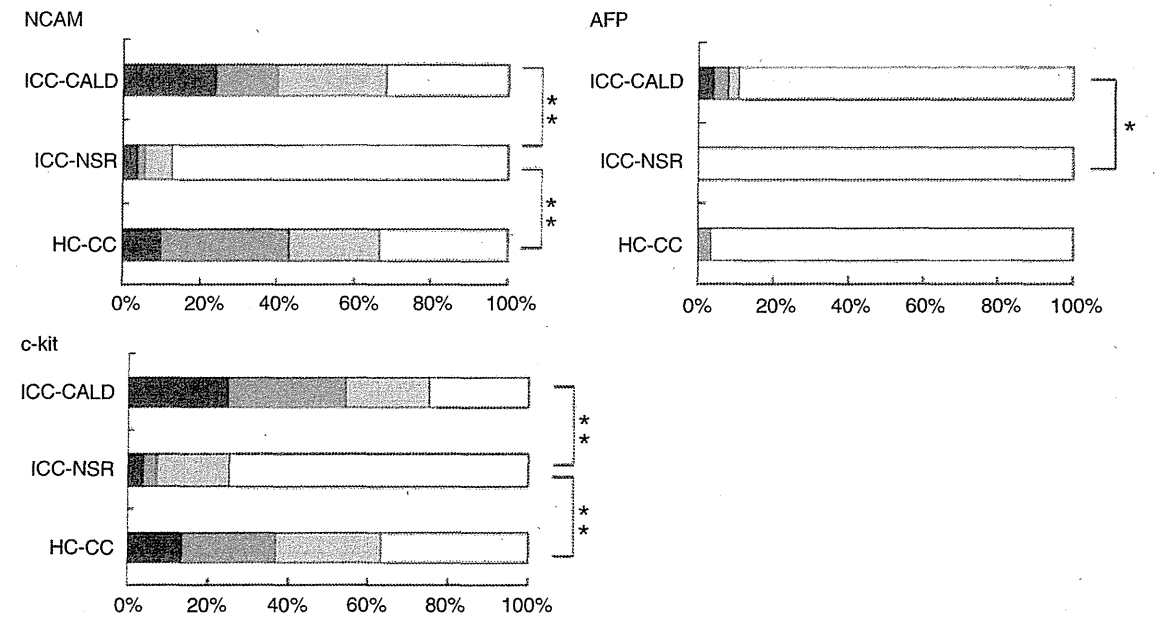

Figure 4. Expression of neural cell adhesion molecule (NCAM), c-Kit and α-fetoprotein (AFP) in intrahepatic cholangiocarcinoma (ICC) with chronic advanced liver disease (CALD), ICC with non-specific reactive changes (NSRs), and combined hepatocellular cholangiocarcinoma (HC-CC). □, negative (0%); ▫, 1–10%; ▩, 11–50%; and ■, >50%; *$P < 0.05$, **$P < 0.001$.

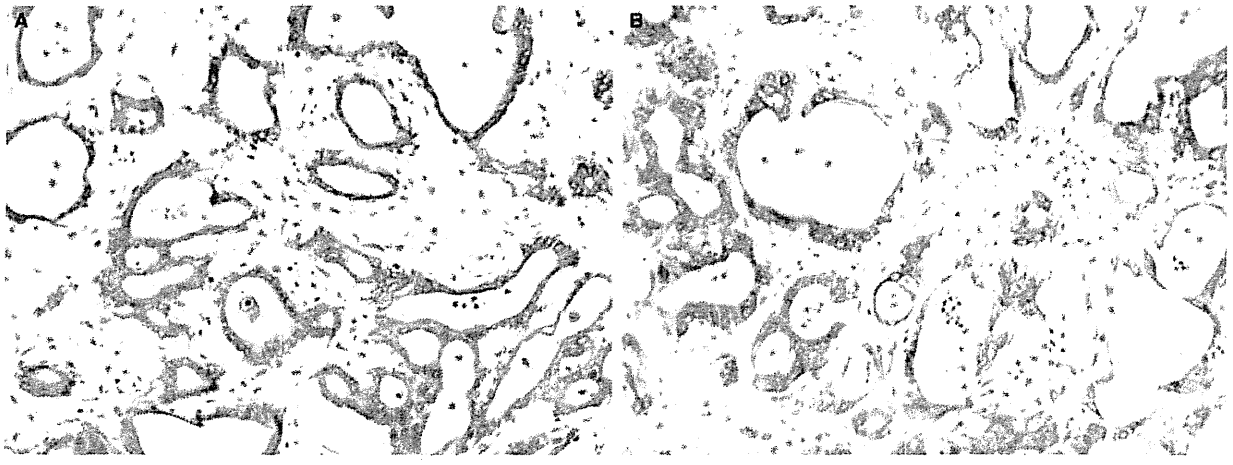

Figure 5. Expression of cytokeratin (CK)7 (**A**) and CK19 (**B**) in intrahepatic cholangiocarcinoma with non-specific reactive changes of the liver. Immunostaining of CK7 and CK19 with haematoxylin.

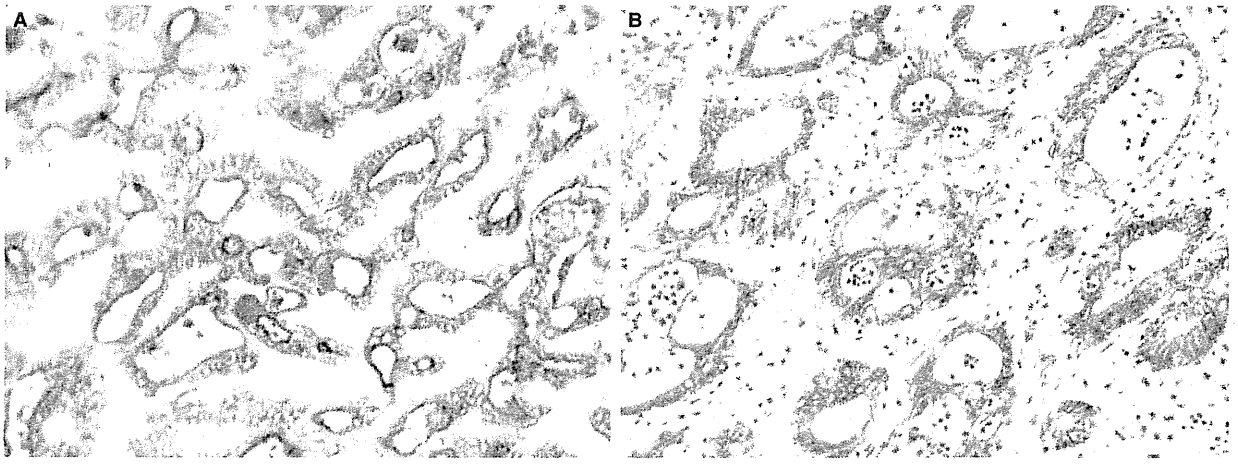

Figure 6. Expression of epithelial membrane antigen (EMA) (**A**) and epithelial cell adehesion molecule (EpCAM) (**B**) in intrahepatic cholangiocarcinoma with non-specific reactive changes of the liver. Immunostaining of EMA and EpCAM with haematoxylin, ×200.

ICC with NSR changes and in ICC with CALD, reaching 97% and 99%, respectively (Figure 6B). Regarding the CC component of HC-CC, 23 (77%) of 30 cases expressed EpCAM. EpCAM expression was lower in the CC component of HC-CC than in ICC with NSR changes ($P < 0.05$).

Expression of NCAM and c-Kit

NCAM. NCAM was expressed with a membranous and, to a lesser degree, cytoplasmic pattern in carcinoma cells (Figure 7). NCAM was expressed in only 11 (15%) of 72 ICCs with NSR changes, but more frequently in ICCs with CALD (75% of 71 cases) and in the CC component of HC-CC (67% of 30 cases) ($P < 0.001$). No difference in NCAM expression was observed between ICC with CALD and the CC component of HC-CC.

c-Kit. c-Kit was expressed diffusely in the cytoplasm or the membrane as well as in the inflammatory cells. Expression of c-Kit in ICC with CALD (82% of 71 cases) and the CC component of HC-CC (63% of 30 cases) was frequent in comparison with ICC with NSR changes (17% of 72 cases) (Figure 8A). c-Kit was also expressed in the HCC component in 20% of 30 cases of HC-CC.

Expression of HepPar 1 and AFP

HepPar 1. In the carcinoma cells of ICC with NSR changes and ICC with CALD, and also in those of the

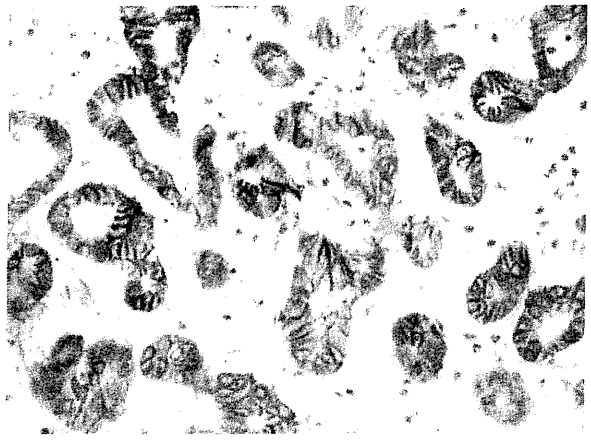

Figure 7. Expression of neural cell adehesion molecule (NCAM) in intrahepatic cholangiocarcinoma with chronic advanced liver disease. Immunostaining of NCAM with haematoxylin.

ICC component of HC-CC, HepPar 1 was negative. In contrast, the HCC component of HC-CC was positive for HepPar 1 in 16 (53%) of 30 cases (data not shown).

AFP. In the HCC component of HC-CC, AFP was expressed in seven (23%) of 30 cases. In one of 30 HC-CC cases, AFP was expressed focally in the CC component (Figure 4). In contrast, none of 72 cases of ICC with NSR changes was positive for AFP. AFP was expressed in carcinoma cells of eight (11%) of 71 ICCs with CALD, including three cases with a diffusely cytoplasmic staining pattern and five cases showing focal or moderate staining (Figure 8B).

CULTURES

Western blotting showed that EpCAM was expressed in all six CC cell lines, but not in the PLC5 HCC cell line (Figure 9). The level of EpCAM expression varied among the EpCAM-producing cell lines; it was highest in CCKS-1, but lowest in SSP-25. Among the three isoforms of NCAM with molecular masses of 120, 140 and 180 kDa, only the 140-kDa isoform was observed in RBE; however, it was expressed weakly. CK19 expression was easily identified in all of the cell lines; however, it was relatively weak in PLC5. Furthermore, AFP expression was only observed in PLC5, and was intense.

Discussion

The findings of this study can be summarized as follows: (i) the expression of mucin was higher in ICC with NSR changes, but relatively low in ICC with CALD and the CC component of HC-CC; (ii) the levels of CK7, CK19, EMA and EpCAM were lower in the CC component of HC-CC than in ICC with NSR changes – the levels of these molecules in ICC with CALD were between these two; (iii) ICC with CALD and the CC component of HC-CC showed higher expression of NCAM and c-Kit, whereas the expression of these molecules was lower in ICC with NSR changes; (iv) AFP was occasionally expressed in ICC with CALD and the CC component of HC-CC, but was absent in ICC

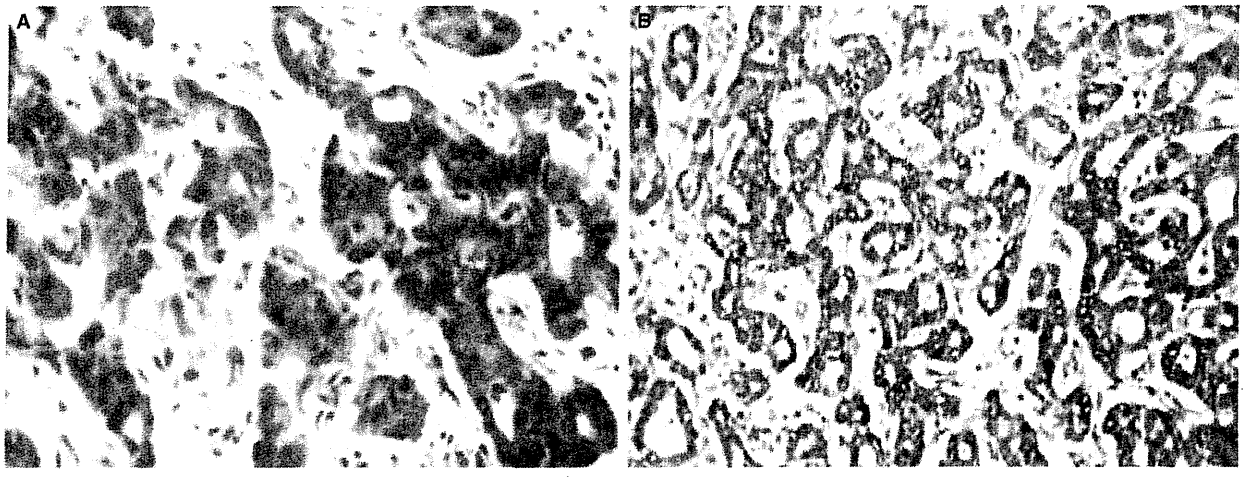

Figure 8. Expression of c-Kit (A) and α-fetoprotein (AFP) (B) in intrahepatic cholangiocarcinoma with chronic advanced liver disease. Immunostaining of c-Kit and AFP with haematoxylin.

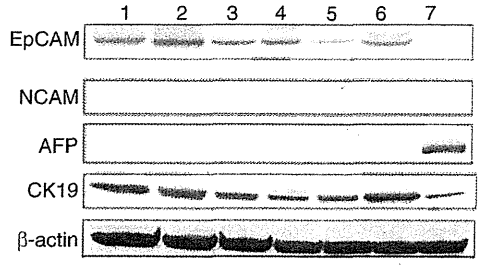

Figure 9. Western blot: expression of biliary epithelial markers [epithelial cell adhesion molecule (EpCAM) and cytokeratin (CK)19], hepatic progenitor cell markers [neural cell adhesion molecule (NCAM)] and hepatocellular or hepatocellular carcinoma (HCC) markers [α-fetoprotein (AFP)] in six cholangiocarcinoma (CC) cell lines (lanes: 1, HuCCT; 2, CCKS-1; 3, IHGGK; 4, RBE; 5, SSP-25; and 6, TKKK) and one HCC cell line (lane 7: PLC5). EpCAM is expressed in all six CC cell lines, but not in the PLC5 HCC cells. NCAM is weakly expressed only in RBE (lane 4). CK19 is expressed in all CC cell lines and one HCC cell line. AFP expression is observed only in PLC5 (lane 7).

with NSR changes; and (v) EpCAM and CK19 were constantly expressed in cultured CC cells, whereas NCAM was infrequently expressed in cultured CC cells.

The production of mucin and the expression of biliary epithelial phenotypes are common in cases of ICC.[2,3] It was found in this study that mucin production as shown by AB and dPAS staining in carcinoma cells was frequent and extensive in ICC with NSR changes in comparison with ICC with CALD and the CC component of HC-CC. Immunohistochemically, the expression of CK7, CK19, EMA and EpCAM, which are known markers of biliary epithelial differentiation,[7,11,15,18] was frequent and extensive in ICC with NSR changes, but relatively infrequent and low in the CC component of HC-CC. Although there were no significant differences in the frequency or extent of expression of these biliary markers between ICC with CALD and ICC with NSR changes, the extent of expression was less in the former than in the latter. In fact, EpCAM and CK19 were constantly and strongly expressed in all six cell lines of CC (HuCCT1, CCKS-1, IHGGK, RBE, SSP-25, and TKKK). It therefore seems plausible that the biliary epithelial phenotypes of carcinoma cells characterized by mucin production and expression of CK7, CK19, EMA and EpCAM in ICC with CALD were similar to those of the CC component of HC-CC and rather different from those of ICC with NSR changes.

Recent studies have shown that HPCs, which exist in bile ductules and/or canals of Hering, can differentiate into hepatocytes and cholangiocytes,[7,19–21] and are activated in most cases of chronic liver disease. Interestingly, HPCs are potential targets for carcinogenesis and, eventually, primary liver tumours with features of HPC may develop.[8,9,22] NCAM, a surface glycoprotein belonging to the immunoglobulin superfamily, is expressed in biliary cells at an early developmental stage (ductal plate), but gradually disappears with the maturation of the bile duct.[19] Canals of Hering and proliferating or reactive bile ductules are reported to express NCAM, and are regarded as candidates for proliferating HPCs.[19,23,24,25] The *c-kit* gene, a proto-oncogene encoding a transmembrane tyrosine kinase receptor, is known to be a haematopoietic stem cell marker.[10,11,15] c-Kit-expressing cells have the capacity to differentiate into the biliary epithelial cell lineage, and, in diseased human livers, canals of Hering and proliferating HPCs are known to express c-Kit; c-Kit is therefore regarded as a marker for HPCs.[10,11]

It was found in this study that, in ICCs with CALD and the CC component of HC-CC, NCAM was expressed in 75% and 67% of cases examined, respectively, but among ICCs with NSR changes, only a small proportion (15%) expressed NCAM, suggesting that ICC with CALD and the CC component of HC-CC bear common features of HPCs. Cell culture experiments showed that only one (RBE) of six CC cell lines expressed NCAM. Furthermore, c-Kit was also frequently expressed in ICC with CALD (83%) and the CC component of HC-CC (63%), whereas such expression was low in ICC with NSR changes (18%). Taken together, these findings show that ICC with CALD and the CC component of HC-CC share frequent expression of the features or phenotype of HPCs, whereas this phenotype is relatively infrequent in ICC with NSR changes.

Although AFP is often used as a tumour marker for HCC, it is also one of the earliest markers detected in the liver bud,[26,27] and the expression of AFP has been found in hepatoblasts and, to a lesser extent, in committed hepatocytic progenitors.[28] If AFP-producing cells are present in ICC, it seems likely that they differentiate into the hepatocellular lineage.[28] In the present study, in eight (11%) of 71 ICCs with CALD and in one (3.3%) of 30 HC-CC cases, AFP was detected in a minor population of CC cells that were negative for HepPar 1, suggesting that these ICC cells may reflect hepatocellular differentiation. AFP expression was absent in ICC with NSR changes, and cultures also failed to detect AFP expression in the six CC cell lines. These findings also suggest that ICC with CALD and the CC component of HC-CC share occasional expression of AFP.

Taking these findings together, it seems likely that ICC with CALD and the CC component of HC-CC share histological features and phenotypes, including features of HPCs. HC-CC is known to develop frequently in cases of CALD, usually in relation to a hepatitis virus infection, and this was also the case in this study. The association

with CALD may be at least partly responsible for the features of HPCs and the relatively low levels of mucin and biliary epithelial markers in the CC component of both HC-CC and ICC with CALD. Such a frequent association with CALD is also seen in other primary liver tumours with progenitor cell features.[24,29]

It has long been controversial whether hepatic malignancies arise from stem cells or HPCs that undergo a malignant transformation or from the dedifferentiation of neoplastically transformed mature hepatocytes.[8,9,22] According to recent studies, HC-CC originates from the transformation of HPCs.[12] Therefore, the following cholangiocarcinogenesis is likely in ICC with CALD. HPCs may undergo either hepatocellular and biliary differentiation or biliary differentiation. The former may be followed by the development of HC-CC, whereas the latter may be followed by the development of ICC. On the other hand, ICC with CALD might be derived from HC-CC, which originates from HPCs at the first step, with ultimate induction of the CC phenotype.

In conclusion, ICC with CALD and the CC component of HC-CC share several common phenotypes, and, in this context, seem to be different from ICC with NSR changes. Such phenotypes include relatively less expression of mucin and biliary markers, but relatively frequent expression of HPC or bile ductular phenotypes such as NCAM and c-Kit. In fact, AFP was also occasionally expressed in ICC with CALD and the CC component of HC-CC. HPCs may be involved in cholangiocarcinogenesis in CALD, as speculated for HC-CC.

References

1. Nakanuma Y, Sasaki M, Ikeda H *et al.* Pathology of peripheral intrahepatic cholangiocarcinoma with reference to tumorigenesis. *Hepatol. Res.* 2008; **38**; 325–334.
2. Nakanuma Y, Harada K, Ishikawa A, Zen Y, Sasaki M. Anatomic and molecular pathology of intrahepatic cholangiocarcinoma. *J. Hepatobiliary Pancreat. Surg.* 2003; **10**; 265–281.
3. Malhi H, Gores GJ. Cholangiocarcinoma: modern advances in understanding a deadly old disease. *J. Hepatol.* 2006; **45**; 856–867.
4. Reddy SB, Patel T. Current approaches to the diagnosis and treatment of cholangiocarcinoma. *Curr. Gastroenterol. Rep.* 2006; **8**; 30–37.
5. Ikai I, Arii S, Ichida T *et al.* Report of the 16th follow-up survey of primary liver cancer. *Hepatol. Res.* 2005; **32**; 163–172.
6. Kubo S, Uenishi T, Yamamoto S *et al.* Clinicopathologic characteristics of small intrahepatic cholangiocarcinomas of mass-forming type. *Hepatol. Res.* 2004; **29**; 223–227.
7. Roskams TA, Theise ND, Balabaud C *et al.* Nomenclature of the finer branches of the biliary tree: canals, ductules, and ductular reactions in human livers. *Hepatology* 2004; **39**; 1739–1745.
8. Roskams T. Progenitor cell involvement in cirrhotic human liver diseases: from controversy to consensus. *J. Hepatol.* 2003; **39**; 431–434.
9. Roskams TA, Libbrecht L, Desmet VJ. Progenitor cells in diseased human liver. *Semin. Liver Dis.* 2003; **23**; 385–396.
10. Crosby HA, Kelly DA, Strain AJ. Human hepatic stem-like cells isolated using c-kit or CD34 can differentiate into biliary epithelium. *Gastroenterology* 2001; **120**; 534–544.
11. Crosby HA, Nijjar SS, de Goyet Jde V, Kelly DA, Strain AJ. Progenitor cells of the biliary epithelial cell lineage. *Semin. Cell Dev. Biol.* 2002; **13**; 397–403.
12. Zhang F, Chen XP, Zhang W *et al.* Combined hepatocellular cholangiocarcinoma originating from hepatic progenitor cells: immunohistochemical and double-fluorescence immunostaining evidence. *Histopathology* 2008; **52**; 224–232.
13. Saito K, Minato H, Kono N *et al.* Establishment of the human cholangiocellular carcinoma cell line (CCKS1). *Kanzo* 1993; **34**; 122–129.
14. Sugawara H, Yasoshima M, Katayanagi K *et al.* Relationship between interleukin-6 and proliferation and differentiation in cholangiocarcinoma. *Histopathology* 1998; **3**; 145–153.
15. Yamashita T, Ji J, Budhu A *et al.* EpCAM-positive hepatocellular carcinoma cells are tumor-initiating cells with stem/progenitor cell features. *Gastroenterology* 2009; **136**; 1012–1024.
16. Li WL, Su J, Yao YC *et al.* Isolation and characterization of bipotent liver progenitor cells from adult mouse. *Stem Cells* 2006; **24**; 322–332.
17. Ishii T, Yasuchika K, Suemori H, Nakatsuji N, Ikai I, Uemoto S. Alpha-fetoprotein producing cells act as cancer progenitor cells in human cholangiocarcinoma. *Cancer Lett.* 2010; **294**; 25–34.
18. de Boer CJ, van Krieken JH, Janssen-van Rhijn CM, Litvinov SV. Expression of Ep-CAM in normal, regenerating, metaplastic, and neoplastic liver. *J. Pathol.* 1999; **188**; 201–206.
19. Roskams T. Liver stem cells and their implication in hepatocellular and cholangiocarcinoma. *Oncogene* 2006; **25**; 3818–3822.
20. Theise ND, Saxena R, Portmann BC *et al.* The canals of Hering and hepatic stem cells in humans. *Hepatology* 1999; **30**; 1425–1433.
21. Libbrecht L. Hepatic progenitor cells in human liver tumor development. *World J. Gastroenterol.* 2006; **12**; 6261–6265.
22. Libbrecht L, De Vos R, Cassiman D, Desmet V, Aerts R, Roskams T. Hepatic progenitor cells in hepatocellular adenomas. *Am. J. Surg. Pathol.* 2001; **25**; 1388–1396.
23. Kozaka K, Sasaki M, Fujii T *et al.* A subgroup of intrahepatic cholangiocarcinoma with an infiltrating replacement growth pattern and a resemblance to reactive proliferating bile ductules: 'bile ductular carcinoma'. *Histopathology* 2007; **51**; 390–400.
24. Kim H, Park C, Han KH *et al.* Primary liver carcinoma of intermediate (hepatocyte–cholangiocyte) phenotype. *J. Hepatol.* 2004; **40**; 298–304.
25. Baumann U, Crosby HA, Ramani P, Kelly DA, Strain AJ. Expression of the stem cell factor receptor c-kit in normal and diseased pediatric liver: identification of a human hepatic progenitor cell? *Hepatology* 1999; **30**; 112–117.
26. Zaret KS. Regulatory phases of early liver development: paradigms of organogenesis. *Nat. Rev. Genet.* 2002; **3**; 499–512.
27. Shafritz DA, Oertel M, Menthena A, Nierhoff D, Dabeva MD. Liver stem cells and prospects for liver reconstitution by transplanted cells. *Hepatology* 2006; **43**; S89–S98.
28. Schmelzer E, Wauthier E, Reid LM. The phenotype of pluripotent human hepatic progenitors. *Stem Cells* 2006; **24**; 1852–1858.
29. Sasaki M, Tsuneyama K, Ishikawa A, Nakanuma Y. Intrahepatic cholangiocarcinoma in cirrhosis presents granulocyte and granulocyte-macrophage colony-stimulating factor. *Hum. Pathol.* 2003; **34**; 1337–1344.

Pathology International

Pathology International 2011; **61**: 773–777 doi:10.1111/j.1440-1827.2011.02738.x

Case Report

Intraductal papillary neoplasm arising from peribiliary glands connecting with the inferior branch of the bile duct of the anterior segment of the liver

Yoshitsugu Nakanishi,[1,4] Yasuni Nakanuma,[5] Masanori Ohara,[1] Toshiyasu Iwao,[2] Noriko Kimura,[3] Takuzo Ishidate[3] and Hiroshi Kijima[6]

Departments of [1]Surgery and [2]Gastrointestinal Medicine and [3]Surgical Pathology, National Hospital Organization, Hakodate Hospital, Hakodate, and [4]Department of Surgical Oncology, Hokkaido University Graduate School of Medicine, Sapporo, and [5]Department of Human Pathology, Kanazawa University Graduate School of Medicine, Kanazawa, and [6]Department of Pathology and Bioscience, Hirosaki University Graduate School of Medicine, Hirosaki, Japan

Intraductal papillary neoplasms of the bile duct are generally thought to arise from neoplastic papillary proliferation of epithelial cells lining the bile duct. We herein report a case with findings that strongly suggested that the biliary cystic tumor might have derived from a peribiliary gland. A 69-year-old female was found to have a cystic lesion with intracystic protrusions at the anterior segment of the right hepatic lobe and underwent hepatic anterior segment resection. Fluoroscopy of the resected specimen injected with contrast medium into the cyst revealed a connection between the cystic lesion and the bile ducts. The cyst was multilocular in appearance. On microscopic examination, the cyst was located within the portal tract of the inferior branch of the anterior segment and connected with the inferior branch of the bile duct. The wall of the hepatic cyst lacked an ovarian-like stroma. The tumor was composed of papillary and glandular components, and the tumor cells were similar to gastric foveolar and pyloric gland epithelia and regarded as adenoma. These tumor cells were positive for MUC 5AC, MUC6, and HIK1083. The tumor was finally diagnosed as an intraductal papillary neoplasm of the bile duct (adenoma, gastric type) arising from a peribiliary gland.

Key words: biliary cystic tumor, gastric type, intraductal papillary neoplasm of the bile duct, peribiliary gland

According to the World Health Organization (WHO) classification of tumors of the digestive system, hepatic or biliary cystic tumors are generally divided into mucinous cystic neoplasms (MCN) and intraductal papillary neoplasms of the bile duct (IPNB).[1,2] MCN are characterized by neoplastic proliferation of cyst-lining epithelia and ovarian-like stroma in the cyst wall and occur only in females.[1] In addition, this type usually lacks a luminal communication to the bile duct lumen.[1,2] In contrast, IPNBs have a luminal communication with the bile duct and show neoplastic papillary proliferation of the biliary epithelial cells and variable dilatation, not infrequently cystic dilatation, of the affected bile ducts.[3,4] Zen *et al.* analyzed nine IPNB cases.[5] In contrast to hepatic MCN, these nine cases lacked ovarian-like stroma in the wall, and they occurred in both sexes. Therefore, IPNBs might arise from a different developmental pathway than hepatic MCN; they are generally thought to arise from neoplastic papillary proliferation of epithelial cells lining the bile duct.[1,2,5]

A case with findings that strongly suggested that the biliary cystic tumor might have derived from a peribiliary gland is reported.

CLINICAL SUMMARY

A 69-year-old woman was found to have a cystic lesion in the anterior segment of the right lobe of the liver. Because the cystic lesion was increasing in size and there were protrusions in the cyst, she was admitted to our hospital.

Pre-surgical operation imaging

Dynamic CT and gadoxetic acid-enhanced magnetic resonance imaging (MRI) showed a cystic lesion at the confluence

Correspondence: Yoshitsugu Nakanishi, MD, Department of Surgery, National Hospital Organization, Hakodate Hospital, 18-16 Kawahara-cho, Hakodate 041-8512, Japan. Email: y.nakanishi@mac.com

Received 10 June 2011. Accepted for publication 15 August 2011.

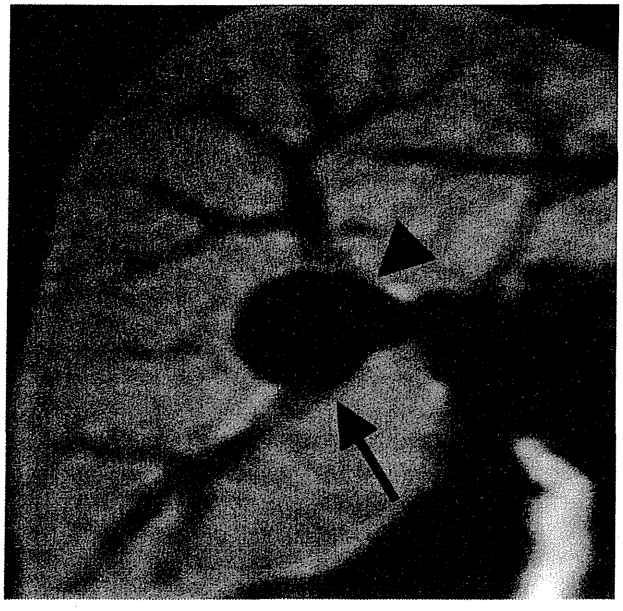

Figure 1 The coronal section view of magnetic resonance imaging (MRI) shows a cystic lesion at the confluence of the superior and inferior branches of the bile ducts of the anterior segment.

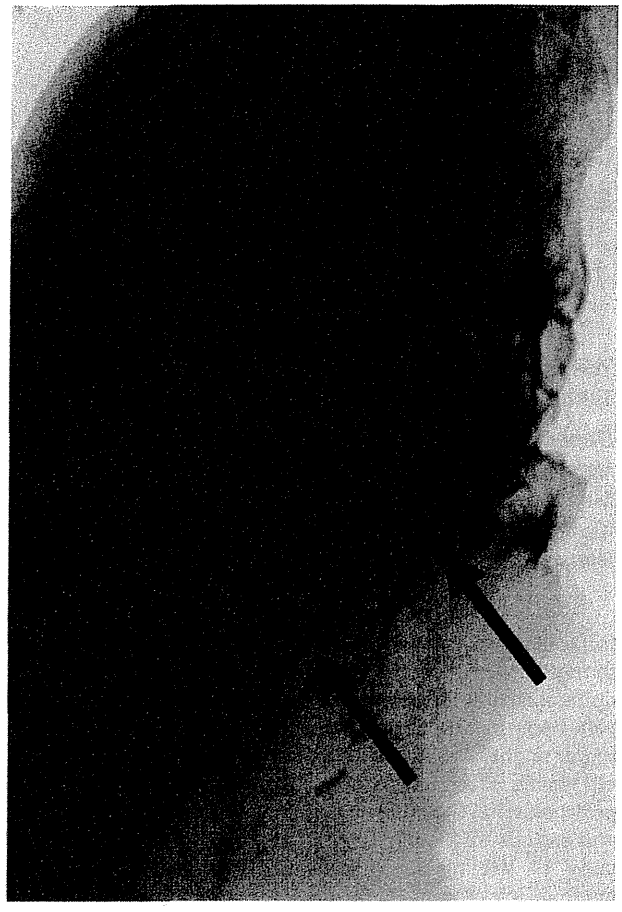

Figure 2 Fluoroscopy of the resected liver specimen injected with contrast medium into the cystic space. The cyst and the surrounding bile ducts are visualized on fluoroscopy, suggesting a direct luminal communication between the confluence of the bile ducts of the anterior segments of the liver and the cyst. The arrowhead and the arrow show the superior and the inferior branches of the bile ducts of the anterior segment, respectively.

of the anterior superior and inferior bile ducts of the right hepatic lobe. (Fig. 1) The proximal and distal bile ducts from the cystic lesion showed no abnormalities, such as dilation, exclusion, or stenosis. Endoscopic retrograde cholangiography revealed that the major intrahepatic bile ducts appeared normal, but it failed to reveal the cystic lesion. From the above findings, it could not be determined whether the cystic lesion was IPNB with cystic change or hepatic MCN, and surgical resection of the anterior segment of the right hepatic lobe was performed. No recurrence has been observed 12 months after surgical resection.

Pathological findings

Immediately after surgical resection, formalin was injected into the cystic lesion, and it was found that formalin was discharged from the margin of the anterior bile duct. In addition, contrast medium was injected into the cystic lesion, and the communication was examined by fluoroscopy. The bile ducts of the anterior segment were visualized in addition to the cystic space, suggesting that the cystic tumor communicated directly with the lumen of the adjacent bile duct. (Fig. 2)

Many serial sections at 5–6 mm intervals were prepared from the surgically resected specimen to examine the drainage of formalin injected into the cystic tumor and the relationship between the cystic tumorous lesion and the anterior bile ducts. Macroscopic examination revealed that the cystic lesion was located within the portal tract of the inferior branch of the anterior segment. The cystic tumor, measuring 1.6 cm × 1.4 cm, showed a multilocular appearance, and a few papillary nodules, 0.4–0.9 cm in diameter, protruded from the wall of the cyst. This tumor was very close to the bile duct.

On microscopic examination, the cystic tumor was located in the portal tract and connected to the inferior branch of the bile duct of the anterior segment (Fig. 3a). The cyst tumor was multilocular, and the cyst wall was composed of thin fibrous connective tissue and lacked ovarian-like stroma; instead, there were many peribiliary glands around the cystic tumor and some glandular components, such as a dilated peribiliary gland with atypical epithelium in the wall of the cyst (Fig. 3b).

The cyst was lined by neoplastic papillary and glandular components. Tumor cells were similar to gastric pyloric gland and foveolar epithelia. A major part of the inner cyst wall was

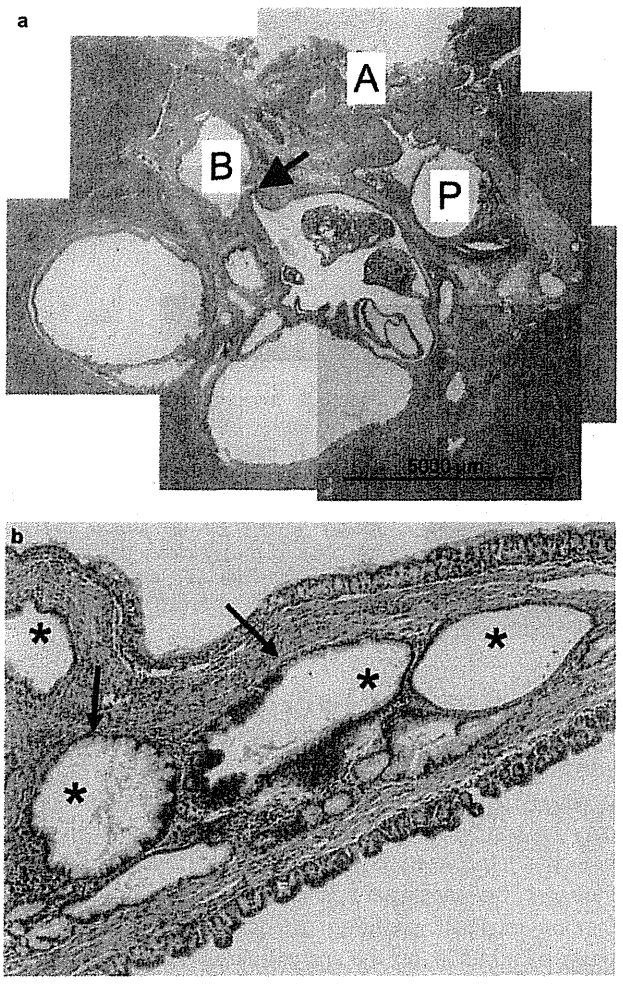

Figure 3 Microscopic findings of the cystic tumor. (**a**) The portal tract of the inferior branch of the anterior segment of the liver. The cystic tumor is multilocular and located within the portal tract, adjacent to the inferior branch of the bile duct (B). Papillary projections from the cyst wall are found. A, the artery. P, the portal vein. The arrow, the connection site between the cystic tumor and the inferior branch of the bile duct. (HE). (**b**) Glandular components of dilated peribiliary glands (*) are present, and some of them are replaced by neoplastic atypical epithelium (arrows) (HE).

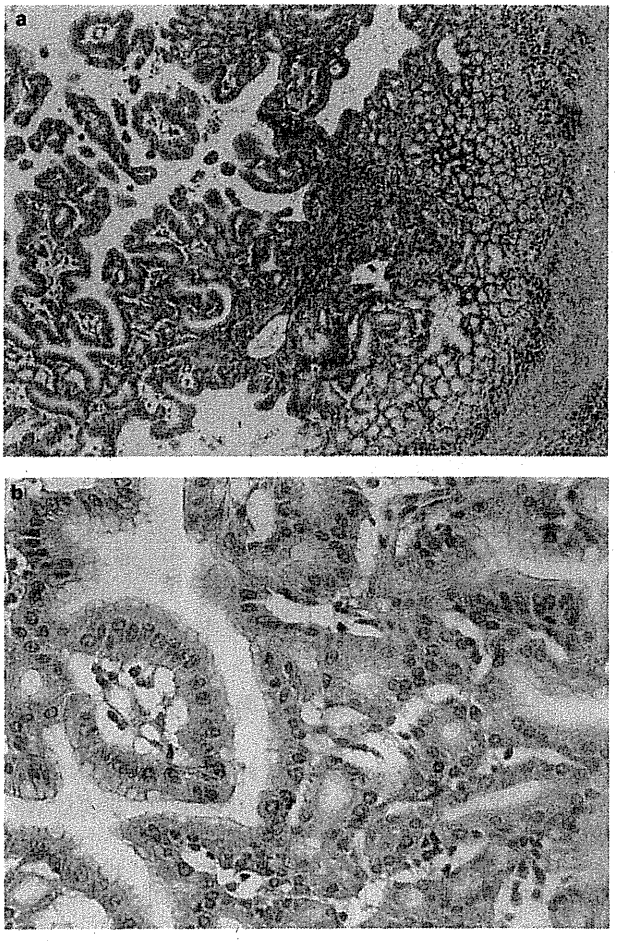

Figure 4 Microscopic findings of the cystic tumor. (**a**) Papillary projections of the tumor show papillo-tubular (left side) and glandular (right side) configurations, similar to gastric foveolar and pyloric epithelia, respectively (HE). (**b**) The atypical grade of the tumor cells (similar to gastric pyloric epithelium) is not high, so this tumor is diagnosed as adenoma (HE).

covered with atypical epithelium, which was similar to gastric pyloric gland epithelium (Fig. 4a). Atypical epithelium similar to gastric foveolar epithelium was primarily present in the papillo-tubular components (Fig. 4a). The atypical grade of the tumor cells was low. Therefore, the tumor grade was diagnosed as adenoma (Fig. 4b).

Immunohistochemical staining for MUC1 (clone Ma695; Novocastra Laboratories, Newcastle, UK), MUC2 (clone Ccp58; Novocastra), MUC5AC (clone CLH2; NovoCastra), MUC6 (clone CLH5; NovoCastra), and HIK 1083 (Kanto Chemical Co., Inc. Tokyo, Japan) was performed with the automated immunostainer (BenchMark platform, Ventana Medical Systems, Inc., Tucson, AZ, USA). The tumor cells were negative for MUC1 and MUC2, but atypical cells similar to gastric foveolar cells were mainly positive for MUC5AC (Fig. 5a), and those similar to pyloric gland cells were mainly positive for MUC6 (Fig. 5b) and HIK1083 (Fig. 5c), which are specific for gastric pyloric glands. In addition, normal peribiliary glands were also positive for MUC6 and HIK1083, but the bile ducts were negative for MUC6 and HIK1083 (Fig. 5d).

From these findings, particularly the close location of this cystic tumor to the bile duct and the presence of peribiliary glands around the tumor, the cystic tumor was finally diagnosed as IPNB (adenoma, gastric type),[1,2] probably arising from peribiliary glands at the confluence of the superior and inferior bile ducts of the anterior segment of the right hepatic lobe.

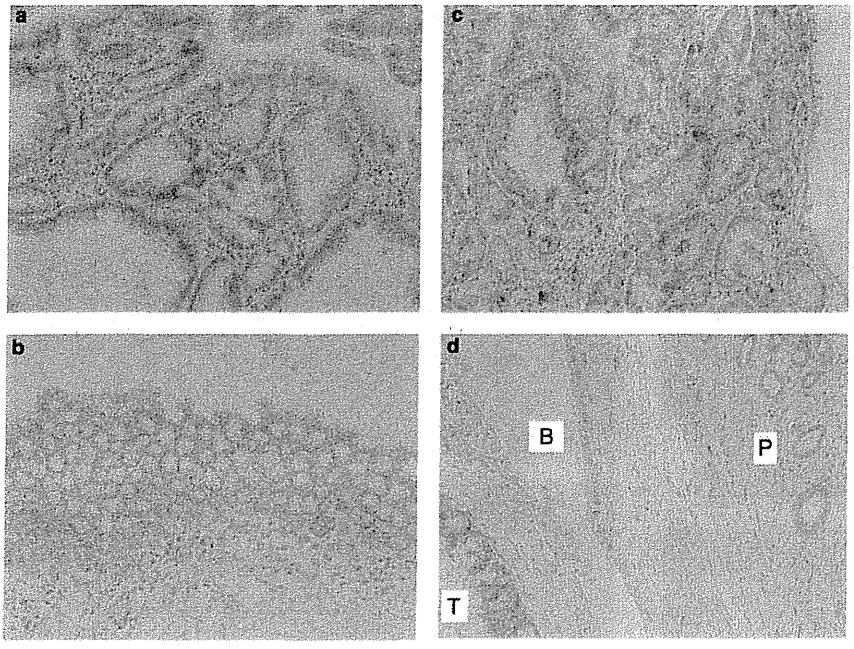

Figure 5 Immunohistochemical staining for the tumor. (**a**) Tumor cells similar to gastric foveolar epithelium are mainly positive for MUC5AC and tumor cells similar to gastric pyloric epithelium are mainly positive for (**b**) MUC6 and (**c**) HIK1083; (**d**) the peribiliary glands (P) and tumor epithelium (T) are positive for MUC6, but the epithelium of the bile duct (B) is negative.

DISCUSSION

This case demonstrates several characteristics: (i) the cystic tumor was incidentally found radiologically, and its size was small; (ii) the cystic lesion was located within periductal connective tissue around the large intrahepatic bile duct; (iii) direct luminal communication of the cystic tumor with the large bile duct was shown, but the large bile ducts around this cystic lesion were not affected radiologically, and the epithelium lining the bile ducts did not show neoplastic change on pathological examination; (iv) the appearance of the tumor was multilocular and ovarian-like stroma was absent beneath the wall; and (v) the tumor was positive for MUC6 and HIK1083.

The bile ducts as the origin of the present tumor were puzzling. If the present tumor had originated from the large bile duct in the portal tract near the confluence of the inferior and superior branches of the anterior segment, the intrahepatic bile ducts would have shown changes such as dilation of the proximal bile ducts on preoperative images; however, preoperative images did not show any such changes. Therefore, we concluded that the origin of the present tumor was not the large bile ducts in the portal tract near the confluence of the inferior and superior branches of the anterior segment.

Peribiliary glands are physiologically distributed around the extrahepatic bile duct and large intrahepatic bile ducts (hepatic duct, segment duct, area duct).[6,7] They are histologically classified as intramural or extramural. Intramural peribiliary glands are scattered within the bile duct walls. Extramural peribiliary glands are located in the periductal connective tissue, representing branched tubuloalveolar seromucous glands draining into large bile duct lumina via their conduits. The location of the tumor and the tiny connection between the tumor and the bile duct were compatible with the hypothesis that the tumor might have arisen from the peribiliary glands. The multilocular appearance of the tumor may be compatible with a neoplastic transformation from branched tubuloalveolar glands of the peribiliary glands. Furthermore, the neoplastic epithelia of the present tumor and the non-neoplastic peribiliary glands around the tumor were positive for MUC6, but the epithelia lining the adjoining large bile ducts were negative for MUC6. Sasaki *et al.* also reported that the peribiliary glands characteristically express MUC6.[8,9] Taken together, it seems likely that the cystic tumor arose from the peribiliary glands and grew in the periductal connective tissue. The communication between the bile duct and the peribiliary glands might have remained after neoplastic transformation of the glands.

Terada *et al.* reported six cases of papillary hyperplasia and four cases of papillary and atypical hyperplasia that co-existed among the extramural peribiliary glands in 799 consecutive autopsy livers without intrahepatic cholangiocarcinoma or metastatic carcinoma.[10] Therefore, they suggested that papillary and atypical hyperplasia of the peribiliary glands may lead to neoplasia and even cholangiocarcinoma. The present case is very unique in that the cystic neoplastic change presumably occurred in the peribiliary glands, and that the large bile ducts connected with the cystic neoplasm were not affected by the neoplastic process, probably because the cystic tumor was at an early stage.

The involvement of peribiliary glands has not been evaluated in the histogenesis and development of IPNB. Previously, we reported one case of IPNB with possible

involvement of peribiliary glands in its development.[11] However, in that previous case, the neoplastic changes were already advanced, and both the bile ducts and peribiliary glands showed neoplastic change, so it was difficult to demonstrate that the cystic neoplasm might have originally affected the peribiliary glands. So far, the case presented here is the first case of IPNB in which the peribiliary glands, but not the epithelium lining the bile duct, are responsible for the development of IPNB with cystic change.

Intraductal papillary neoplasm of the bile duct shares many features with intraductal papillary mucinous neoplasms of the pancreas (IPMN), and IPMN is classified into pancreatic main duct type or branch type.[12,13] IPNB arising from the large bile duct share clinicopathological features with IPMN-Ps from the pancreatic main bile duct, including, for example, high malignant potential and high frequency of pancreatobiliary and intestinal type.[14] On the other hand, the branch type of IPMN-P has a good prognosis, and most of its cells are gastric type.[15] In addition, the branch type of IPMN-P is likely to be multilocular in appearance on imaging findings, as in biliary cystic tumor with ductal communication.[16] The biliary counterpart of the branch type of IPMN-P has not been reported. Zen *et al.* reported that the cellular type of all two biliary cyst adenomas with ductal communication was gastric type, as in the present case.[5] We suggest that a biliary counterpart of IPMN-P includes biliary cyst tumor arising from a peribiliary gland.

Intraductal papillary neoplasm of the bile duct can be histologically classified into four categories based on phenotypes: pancreatobiliary, intestinal, gastric, and oncocytic types.[14] The histological form of the present case was similar to the gastric pyloric gland or foveolar epithelium. The gastric type of IPNB is immunohistochemically characterized by negativity for MUC1 and MUC 2 and positivity for MUC5AC and MUC6.[5] In addition, the present case was strongly positive for HIK1083, which is expressed in gastric pyloric and cardiac glands. From these findings, the present papillary tumor was diagnosed as a gastric type adenoma of IPNB.

In conclusion, the present case is the first report of an IPNB that was a gastric phenotype adenoma, and this IPNB probably arose from the peribiliary gland around the intrahepatic bile duct. Future studies on the biological features of IPNB arising from the peribiliary gland are mandatory.

REFERENCES

1 Tsui WMS, Adsay NV, Crawford JM, Hruban R, Kloppel G, Wee A. Mucinous cystic neoplasms of the liver. In: Bosman FT, Carnerio F, Hruban RH, Theise ND, eds. *WHO Classification of Tumours of the Digestive System World Health Organization Classification of Tumours*, 4th edn. Lyon: IARC Press, 2010; 236–38.

2 Nakanuma Y, Curabo MO, Franceschi S *et al.* Intrahepatic cholangiocarcinoma. In: Bosman FT, Carnerio F, Hruban RH, Theise ND, eds. *WHO Classification of Tumours of the Digestive System World Health Organization Classification of Tumours*, 4th edn. Lyon: IARC Press, 2010; 217–24.

3 Sato M, Watanabe Y, Tokui K *et al.* Hepatobiliary cystadenocarcinoma connected to the hepatic duct: A case report and review of the literature. *Hepatogastroenterology* 2003; **50**: 1621–4.

4 Makino I, Yoshimitsu Y, Sakuma H, Nakai M, Ueda H. A large cystic tumor with bile duct communication originating around the hepatic hilum. *J Gastrointestin Liver Dis* 2010; **19**: 77–80.

5 Zen Y, Fujii T, Itatsu K *et al.* Biliary cystic tumors with bile duct communication: A cystic variant of intraductal papillary neoplasm of the bile duct. *Mod Pathol* 2006; **19**: 1243–54.

6 Terada T, Nakanuma Y, Ohta G. Glandular elements around the intrahepatic bile ducts in man; their morphology and distribution in normal livers. *Liver* 1987; **7**: 1–8.

7 Terada T, Nakanuma Y. Morphological examination of intrahepatic bile ducts in hepatolithiasis. *Virchows Arch A Pathol Anat Histopathol* 1988; **413**: 167–76.

8 Bartman AE, Buisine MP, Aubert JP *et al.* The MUC6 secretory mucin gene is expressed in a wide variety of epithelial tissues. *J Pathol* 1998; **186**: 398–405.

9 Sasaki M, Ikeda H, Nakanuma Y. Expression profiles of MUC mucins and trefoil factor family (TFF) peptides in the intrahepatic biliary system: Physiological distribution and pathological significance. *Prog Histochem Cytochem* 2007; **42**: 61–110.

10 Terada T, Nakanuma Y. Pathological observations of intrahepatic peribiliary glands in 1000 consecutive autopsy livers. II. A possible source of cholangiocarcinoma. *Hepatology* 1990; **12**: 92–7.

11 Nakanishi Y, Zen Y, Hirano S *et al.* Intraductal oncocytic papillary neoplasm of the bile duct: The first case of peribiliary gland origin. *J Hepatobiliary Pancreat Surg* 2009; **16**: 869–73.

12 Adsay NV, Fukushima N, Furukawa T *et al.* Intraductal neoplasms of the pancreas. In: Bosman FT, Carnerio F, Hruban RH, Theise ND, eds. *WHO Classification of Tumours of the Digestive System*, 4th edn. Lyon: IARC Press, 2010; 304–13.

13 Nakanuma Y. A novel approach to biliary tract pathology based on similarities to pancreatic counterparts: Is the biliary tract an incomplete pancreas? *Pathol Int* 2010; **60**: 419–29.

14 Zen Y, Fujii T, Itatsu K *et al.* Biliary papillary tumors share pathological features with intraductal papillary mucinous neoplasm of the pancreas. *Hepatology* 2006; **44**: 1333–43.

15 Ishida M, Egawa S, Aoki T *et al.* Characteristic clinicopathological features of the types of intraductal papillary-mucinous neoplasms of the pancreas. *Pancreas* 2007; **35**: 348–52.

16 Procacci C, Megibow AJ, Carbognin G *et al.* Intraductal papillary mucinous tumor of the pancreas: A pictorial essay. *Radiographics* 1999; **19**: 1447–63.

Liver INTERNATIONAL
OFFICIAL JOURNAL OF THE INTERNATIONAL ASSOCIATION FOR THE STUDY OF THE LIVER

Liver International ISSN 1478-3223

CLINICAL STUDIES

A possible involvement of p62/sequestosome-1 in the process of biliary epithelial autophagy and senescence in primary biliary cirrhosis

Motoko Sasaki, Masami Miyakoshi, Yasunori Sato and Yasuni Nakanuma

Department of Human Pathology, Kanazawa University Graduate School of Medicine, Kanazawa, 920-8640, Japan

Keywords
autophagy – biliary epithelial cell – cellular senescence – p62/sequestosome-1 – primary biliary cirrhosis

Correspondence
Yasuni Nakanuma, Department of Human Pathology, Kanazawa University Graduate School of Medicine, Kanazawa 920-8640, Japan Tel: +81 76 265 2195 Fax: +81 76 234 4229 e-mail: pbcpsc@kenroku.kanazawa-u.ac.jp

Received 17 January 2011
Accepted 2 September 2011

DOI:10.1111/j.1478-3231.2011.02656.x

Abstract

Background and Aims: Given autophagy is involved in the pathogenesis in primary biliary cirrhosis (PBC), we examined an involvement of p62 sequestosome-1 (p62), a specific cargo for autophagy, in the process of autophagy and cellular senescence in PBC. *Methods:* We examined immunohistochemically the expression of p62 in livers taken from patients with PBC (n = 46) and control livers (n = 78) and its colocalization with microtubule-associated proteins-light chain 3β (LC3), lysosome-associated membrane protein-1 (LAMP-1) and senescent markers ($p16^{INK4a}$ and $p21^{WAF1/Cip1}$). We examined the expression of p62 and LC3 in cultured biliary epithelial cells (BECs) treated with various stress. The effect of p62 knockdown with *si*RNA on stress-induced autophagy and cellular senescence was also assessed. *Results:* The expression of p62 was specifically seen in cytoplasmic aggregates in BECs in the inflamed and damaged small bile ducts (SBDs) in PBC, when compared with non-inflamed ones in PBC and in control livers ($P < 0.01$). The co-expression of p62 with LC3, LAMP-1 and senescent markers was seen in the inflamed SBDs in PBC, but the intracytoplasmic localization was different. The expression of p62 and LC3 was significantly upregulated in BECs treated with various stress ($P < 0.01$) and pretreatment with bafilomycin A1 enhanced the accumulation of p62-positive aggregates in BECs with serum deprivation. The knockdown of p62 decreased stress-induced autophagy and cellular senescence. *Conclusion:* The aggregation of p62 is specifically increased in the damage bile ducts in PBC and may reflect dysfunctional autophagy, followed by cellular senescence in the pathogenesis of bile duct lesions in PBC.

Macroautophagy (hereafter referred to as autophagy) is a genetically regulated programme responsible for the turnover of cellular proteins and damaged organelles. This evolutionarily conserved process is characterized by the formation of double membrane cytosolic vesicles, autophagosomes, which sequester cytoplasmic content and deliver it to lysosomes (1–4). Autophagy in human diseases has been highlighted during the last decade (1,2,5) and recent data demonstrated that autophagy is involved in major field of hepatology (6–12). Autophagy and cellular senescence are two distinct cellular responses to stress. Recent studies disclosed that autophagy is induced during the process of senescence and facilitates it (3,4). An appropriate cellular stress response is critical for maintaining tissue integrity and function and for preventing diseases. Cells respond to stress with adaptation, repair and recovery, or are diverted into irreversible cell cycle exit (senescence) or are eliminated through programmed cell death (apoptosis) (4). Cellular senescence is a delayed stress response involving multiple effector mechanisms such as the DNA damage response (13) and the senescence-associated secretion phenotype (14–16).

Primary biliary cirrhosis (PBC) is an organ specific autoimmune disease and presents with chronic, progressive cholestasis and liver failure (17–19). PBC is characterized histologically as a cholangitis of small bile ducts (chronic non-suppurative destructive cholangitis; CNSDC) eventually followed by the extensive loss of small bile ducts (17,20). Although there have been many studies on the immunopathological features (21–23), there remains enigma in the pathogenesis of bile duct lesion in PBC. We have reported cellular senescence of biliary epithelial cells (BECs) with the augmented expression of senescence-associated β-galactosidase (SA-β-gal), $p16^{INK4a}$ and $p21^{WAF1/CIP}$ and telomere shortening in damaged small bile ducts in PBC (24–27) and a possible involvement

of autophagy in the pathogenesis of bile duct lesions in PBC (11).

Sequestosome-1, p62, , is an adaptor protein involved in the delivery of ubiquitin-bound cargo to the autophagosome and regulates the formation of protein aggregates (28–31). In a normal cell, p62 binds proteins with ubiquitin chains and delivers them to the autophagosome. When autophagy is disrupted in several model systems, p62 accumulates with ubiquitin-containing aggregates, a condition reminiscent to that of well-known neurodegenerative disorders (30,32), liver injuries (10,33) and hepatocellular carcinoma (12,34). The ubiquitin-positive aggregates that accumulate in autophagy mutants of flies and mice disappear when p62 is depleted (35,36). Therefore, the accumulation of p62 may reflect dysfunctional autophagy in which the capacity of autophagy is not much enough to process the damaged proteins bound to p62 (10,12,37).

Although the involvement of autophagy and cellular senescence is being clarified (11,24–27), there are no studies addressing the possible role of p62 in the pathogenesis of bile duct lesions in PBC. Since the accumulation of p62 is supposed to reflect dysfunctional autophagy, we hypothesized that p62 may be upregulated by various stresses in BECs and this finding may be similar to BECs in the damaged bile ducts in PBC. We examined an involvement of p62 in the process of autophagy and cellular senescence in PBC. Furthermore, we examined the association of p62 with the process of autophagy and cellular senescence in cultured mouse BECs.

Materials and methods

Human study

Classification of intrahepatic biliary tree

The intrahepatic biliary tree is classified into the intrahepatic large and small bile ducts (septal and interlobular bile ducts) by their size and distributions in the portal tracts (38). Bile ductules, which are characterized by tubular or glandular structures with poorly defined lumen and located at the periphery of the portal tracts (38,39), are not included in the small bile ducts.

Small bile ducts were histologically divided largely into 'inflamed' and non-inflamed. Inflamed bile ducts include the bile ducts showing biliary epithelial damages and being surrounded and occasionally infiltrated by inflammatory cells such as CNSDC in PBC (17) and also the bile ducts embedded in infiltrating lymphoid cells and showing mild epithelial damages in chronic viral hepatitis (CVH) (hepatitis duct lesion).

Liver tissue preparation

A total of 124 liver tissue specimens (all were biopsied or surgically resected) were collected from the liver disease file of our laboratory and affiliated hospitals. The Ethics Committee in Kanazawa University approved this study. The liver specimens enrolled in this study were 46 PBC, 22 CVH, 26 non-alcoholic steatohepatiits (NASH), 10 livers with extrahepatic biliary obstruction (EBO), and 20 'histologically normal' livers. All PBC were from the patients fulfilling the clinical, serological and histological characteristics consistent with the diagnosis of PBC (17). PBC livers were staged histologically (17), and 34 and 12 of PBC were of stages 1, 2 (early PBC) and of stages 3, 4 (advanced PBC) respectively. Eleven CVH were regarded as F0-2 and 11 as F3, 4 respectively (40). Two and 20 of CVH cases were serologically positive for hepatitis B surface antigen and antihepatitis C viral antibody respectively. Causes of EBO were obstruction of the bile duct at the hepatic hilum or the extrahepatic bile ducts, because of carcinoma or stone, and the duration of jaundice was less than 1 month. 'Histologically normal' livers were obtained from surgically resected livers for traumatic hepatic rupture or metastatic liver tumour. The liver tissues used were taken from the part sufficiently away from the trauma and tumour. There was no difference in the expression level of p62 and LC3 between biopsied and surgically resected liver specimens of each disease group in preliminary study. Chemotherapy was not performed before liver resection in all patients with histologically normal liver.

Liver tissue samples were fixed in 10% neutral buffered formalin, and embedded in paraffin. More than twenty serial sections, 4 μm thick, were cut from each block. Several were processed routinely for histopathological study, and the remainder was processed for the following immunohistochemistry.

Immunohistochemistry

We examined immunohistochemically the expression of p62 using the antibodies shown in Table 1, as described previously (25). A similar dilution of the control rabbit Immunoglobulin G (Dako) was applied instead of the primary antibody as negative control. Positive and negative controls were routinely included. Histological analysis was performed in a blinded manner.

Double immunostaining

We also performed double immunostaining for p62 with an autophagy marker LC3, a lysosome-associated membrane protein-1 (LAMP-1), and senescence markers, $p16^{INK4a}$ and $p21^{WAF1/Cip1}$ (Table 1), using eight representative PBC livers and three control livers. In brief, p62 was detected as described above, followed by second staining for either of senescence markers ($p16^{INK4a}$ and $p21^{WAF1/Cip1}$) using Vector Blue Alkaline Phosphatase Substrate Kit (Vector Laboratories, Burlingame, CA, USA). Double immunofluorescence staining for p62 and LC3, or p62 and LAMP-1 was performed using each primary antibody and Alexa-546-labelled an-

Table 1. Primary antibodies used in this study

Primary antibody	Type (clone)	Pretreatment	Dilution	Source
p62	Rabbit poly	eARI-BA (121°C, 5 min)	1:1000	MBL, Nagoya, Japan
LC3	Goat poly	MW-CB (95°C, 20 min)	1:50	Santa-Cruz, Santa-Cruz, CA, USA
LC3	Mouse mono (5F10)	eARI-BA (121°C, 5 min)	1:50	NanoTools, San Diego, CA, USA
LAMP-1	Mouse mono (E-5)	MW-CB (95°C, 20 min)	1:200	Santa-Cruz, Santa-Cruz, CA, USA
LAMP-1	Rat mono		1:100	Santa-Cruz, Santa-Cruz, CA, USA
$p16^{INK4a}$	Mouse mono (JC8)	eARI-BA (121°C, 5 min)	1:100	Neomarkers, Freemont, CA, USA
$p21^{WAF1/Cip1}$	Mouse mono (70)	eARI-BA (121°C, 5 min)	1:100	BD Transduction, San Jose, CA, USA

BA, 0.05M boric acid buffer (pH 8); CB, 0.05M citric buffer (pH 6); eARI, electronic antigen retrieval instrument (pascal, Dako); LAMP-1, lysosome-associated membrane protein-1; LC3, microtubule-associated proteins-light chain 3β; MW, microwave treatment; p62, p62/sequestosome-1.

tirabbit IgG (Molecular probes, Eugene, OR, USA) and Alexa-488-labelled antimouse IgG (Molecular probes), using eight representative PBC livers and three control livers. The sections were then counterstained with 10 μg/ml 4′ and 6-diamidino-2-phenylindole (DAPI) and evaluated under a conventional fluorescence microscope (Olympus, Tokyo, Japan).

Electron microscopy

The method for conventional electron microscopy has been described previously (41). We examined the liver samples from seven patients with PBC and two patients with normal liver.

Culture study

Cell culture and treatments of mouse intrahepatic BECs

Mouse intrahepatic biliary epithelial cells (BECs) were isolated from 8-week-old female BALB/c mice and were purified and cultured as described previously (42). The cell density of the cells was less than 80% during experiments. In several experiments, BECs were treated with hydrogen peroxide (PO, 100 μM for 2 h) or Etoposide (100 μM, Sigma Chemica, Co., St. Louis, MO, USA). In several experiments, 3-methyladenine (3MA, 5 mM, Sigma Chemica, Co.), an inhibitor of the class III phosphatidylinositol 3-kinase complex involved in initial autophagosome formation (43) and Bafilomycin A1 (Baf, 5 nM), which causes lysosomal dysfunction (44), were also used. The treatment with serum deprivation for 4 days did not cause significant level of apoptosis in BECs, compared to control (Fig. S1).

Knockdown of p62 by small interfering RNA

Validated small interfering RNA (*si*RNA) for p62 and negative control *si*RNA were purchased from Santa-Cruz biotech. (Santa-Cruz, CA, USA) and QIAGEN (Hilden, Germany) respectively. One day before transfection, BECs were plated in 35 mm-dishes (5×10^5 cells) or Lab-Tek chambers (5×10^4 cells/well), and then the cells were transiently transfected with either p62 or control siRNA (100 nM) using Lipofectamine RNAiMAX (Invitrogen, Carlsbad, CA, USA) according to the manufacturer's protocol.

Real-time quantitative reverse transcriptase-polymerase chain reaction

Total RNA was extracted from the cells with a QIAGEN RNeasy Mini kit (QIAGEN) according to the manufacturer's protocol. After cDNA was synthesized, quantitative real-time PCR was performed to measure a series of p62 and LC3 and β-actin mRNA according to a standard protocol using the SYBR Green PCR Master Mix (Toyobo, Tokyo, Japan). The primer sequences are as follows; p62, 5′-cgatgactggacacatttgtct, 5′-gtccttcctgtgaggggtct (PCR product, 116bp); LC3 5′-gagacattcgggacagcaat, 5′-gtgggtgcctacgttctcat (137bp); β-actin, 5′-ccaccgatccacacagagta, 5′-ggctcctagcaccatgaaga (143bp). Each experiment was performed twice in triplicate, and the mean was adopted in each experiment.

Immunoblotting

The cell lysate samples (10 μl) were resolved by SDS-PAGE and transferred to a nitrocellulose membrane as described previously (45). After transfer, the membranes were processed for immunoblotting as described previously (45). The primary antibody for LC3 and p62 was described above. Using mouse monoclonal anti-α-tubulin (clone TU-01, Zymed, South San Francisco, CA, USA) α-tubulin was detected. Densitometry of the resulting bands was performed using Image-J software and normalized to the loading control.

Immunofluorescence staining for cultured cells

The BECs growing in a Lab-Tek chamber were fixed and immunostained using the primary antibodies for p62, LC3, or LAMP-1 (Table 1), as described previously (11).

Assay for autophagy

The level of autophagy was assessed by the LC3 puncta formation (46). The number of LC3 puncta per cell was counted using the Image-J software.

Assay for cellular senescence

The SA-β-gal activity was detected by using the senescence detection kit (BioVision, Mountain View, CA, USA) according to manufacturer's protocol (47). The proportion of senescent cells in each condition was assessed at day 4 by counting the percentage of SA-β-gal-positive cells in at least 1 x 10^3 total cells using light microscopy.

Statistical analysis

Statistical analysis for the difference used the Mann–Whitney *U*-test. When the *P* value was less than 0.05, the difference was regarded as significant.

Results

Human study

The accumulation of p62-positive aggregates in the inflamed small bile ducts in PBC

The expression of p62 was absent or faint in control livers (Fig. 1A). Whereas, an accumulation of p62-positive aggregates was specifically seen in BECs in the inflamed and damaged small bile ducts in PBC (Fig. 1B). The accumulation of p62-positive aggregates was seen mainly in the supranuclear region in the inflamed bile ducts in PBC (Fig. 1B). The expression of p62 was significantly more frequent in the inflamed small bile ducts (SBDs) in PBC, when compared with non-inflamed ones in PBC and in control livers ($P < 0.01$) (Table 2).

The co-expression of p62 with LC3 and LAMP-1 in the inflamed small bile ducts in PBC

The accumulation of p62-positive aggregates was seen mainly in the supranuclear region in the inflamed bile ducts in PBC, whereas the expression of LC3, an autophagic marker, was detected in the intracytoplasmic vesicles and some of them were located also in the basal region (Fig. 2A). The colocalization of p62 and LC3 was only focally observed (Fig. 2A).The p62-positive aggregates and LAMP-1-positive vesicles were detected in the inflamed small bile ducts in PBC (Fig. 2B). However, there are few colocalizations of p62 and LAMP-1 (Fig. 2B).

The accumulation of autolysosomes in the damaged small bile duct in PBC

Ultrastructurally, several autophagic vacuoles at different stages were observed in BECs in the damaged small bile duct in PBC (Fig. 3). A part of autolysosomes contained degenerative organelle-like structures and myelin-like lamellae (Fig. 3). Autolysosomes with osmiophilic material were also seen (Fig. 3). These accumulated autolysosomes may be a result of lysosomal dysfunction related to late stage of autophagic process. Mitochondrial damage is also seen in the form of swelling, disorganization of the cristae (Fig. 3). The autophagic vacuoles at different stages and mitochondrial damage were observed in BECs in the damaged small bile ducts in all samples from seven patients with PBC, whereas these findings were not seen in the samples from normal livers.

The co-expression of p62 with senescent markers ($p16^{INK4a}$ and $p21^{WAF1/Cip1}$) in the inflamed small bile ducts in PBC

Double immunostaining revealed that the accumulation of p62-positive aggregates was detected in BECs in the inflamed bile ducts showing the expression of senescent markers $p16^{INK4a}$ in PBC (Fig. 4A). $p21^{WAF1/Cip1}$ was also detected in the inflamed bile ducts, but the colocalization of p62-positive aggregates with $p21^{WAF1/Cip1}$ was not observed in BECs (Fig. 4B). Since $p21^{WAF1/Cip1}$ and $p16^{INK4a}$ are involved in induction and maintenance of senescence respectively (48,49), the closer co-expression of p62 and $p16^{INK4a}$ may indicate that the accumulation of p62 may be more closely associated with the later stage of cellular senescence.

Culture study

Increased expression of p62 and LC3 by various cellular stress in BECs

The mRNA expression of p62 and LC3 was significantly upregulated in cultured BECs treated with various stress ($P < 0.01$) (Fig. 5A). The mRNA expression of p62 and LC3 was much more upregulated in cultured BECs treated with serum deprivation and Baf and 3MA (Fig. 5A). The reason why the mRNA expression level of LC3 was higher in BECs with serum deprivation and 3MA than those with serum deprivation remains unknown. Immunoblotting showed that the protein level of p62 was upregulated in serum deprivation with Baf, in accord with the increased mRNA expression (Fig. 5B). The reason why the protein level expression of p62 was not increased by the treatment with hydrogen peroxide and serum deprivation with 3MA, despite the increased mRNA expression remains unknown. The LC3-II/LC3-I ratio, which indicates the level of autophagy, was upregulated by the treatment hydrogen peroxide, Etoposide and serum deprivation with and without Baf (Fig. 5B). Immunofluorescent staining disclosed that p62 expression was observed as cytoplasmic dots in BEC with various stress (Fig. 5C). The number of p62-positive cytoplasmic dots induced by serum deprivation was decreased by a treatment with 3MA, whereas p62-positive dots induced by serum deprivation were more increased by a treatment with Baf (Fig. 5C).

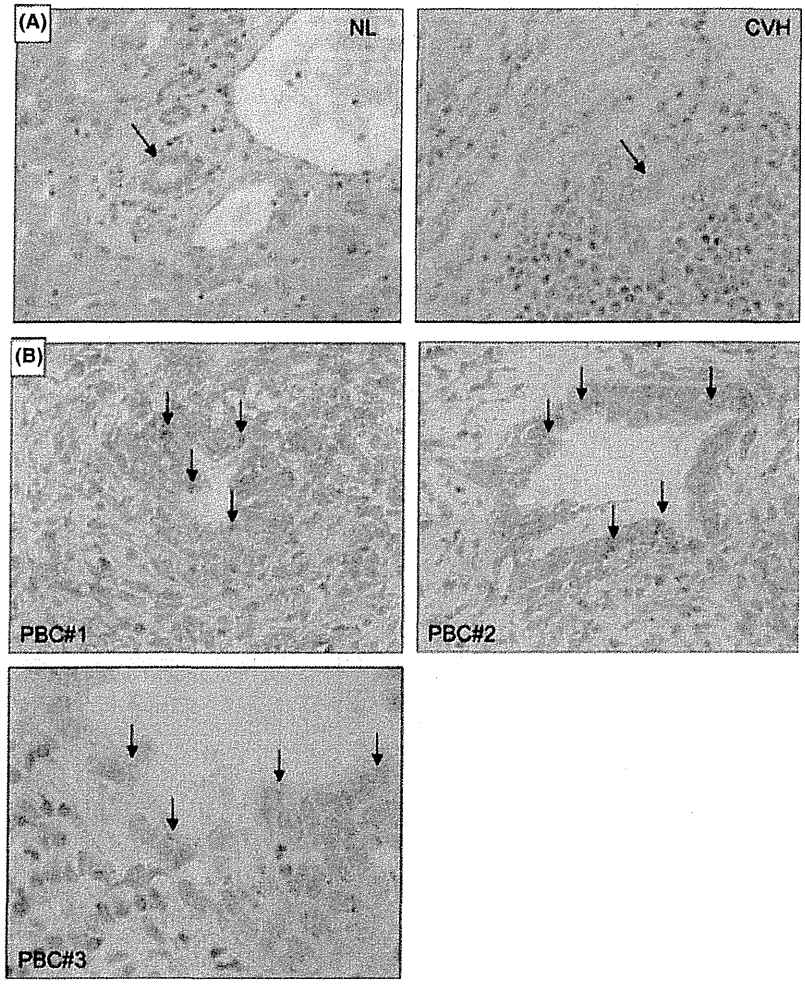

Fig. 1. p62-positive aggregates in the inflamed and damaged small bile ducts in primary biliary cirrhosis (PBC). (A) The expression of p62 was absent in biliary epithelial cells in small bile duct (arrows) in normal liver (NL, left), chronic viral hepatitis (CVH, right). (B) The accumulation of p62-positive aggregates (arrows) was detected mainly in the supranuclear region in the inflamed and damaged small bile duct in PBC. There were several round cells, probably macrophage, in which p62-positive aggregates were seen. PBC cases #1-3 (stage 2). Immunostaining for p62. Original magnification, x400 (PBC#3, x1000).

Co-expression of p62 with LC3 and LAMP-1 in BECs induced by treatments with serum deprivation with and without Bafilomycin A1

The cytoplasmic p62-positive dots and LC3-positive dots were increased, and a part of them was colocalized in BECs treated with serum deprivation (Fig. 6A). The cytoplasmic p62-positive dots and LC3-positive dots induced by serum deprivation were more increased by a treatment with Bafilomycin A1, and there were several p62-positive aggregates in the cytoplasm (Fig. 6A). The cytoplasmic p62-positive dots and LAMP-1-positive dots were increased, and a part of them was colocalized (arrows) in BECs treated with serum deprivation (Fig. 6B). The cytoplasmic p62-positive dots induced by serum deprivation were more increased, whereas and LAMP-1-positive dots were rather decreased by a treatment with Baf (Fig. 6B). There were few yellow dots indicating colocalization of p62 and LAMP-1 in the cytoplasm of the biliary epithelial cells.

The knockdown of p62 results in the inhibition of stress-induced autophagy and cellular senescence

We examined whether or not p62 affects the induction of autophagy and cellular senescence by a knockdown of p62 using *si*RNA. An effective knockdown of p62 using *si*RNA was confirmed in mRNA and protein levels (Fig. 7A). The level of autophagy assessed by LC3 puncta per cell was significantly increased in cells treated with serum deprivation (14.29 ± 4.42), when

Table 2. Frequency of the prevalence of vesicular expression of p62 in small bile ducts in primary biliary cirrhosis and control livers

Diseases	Number of patients	Type of BD	Number of SBD	Number of BD with vesicular p62 expression (%)
PBC	46	Inflamed	149	105 (70.5)*
		Non-inflamed	126	8 (6.3)
CVH	22	Inflamed	173	24 (13.9)†,‡
		Non-inflamed	192	6 (3.1)
NASH	26	Inflamed	16	3 (18.8)†,‡
		Non-inflamed	183	2 (1.1)
EBO	10	Inflamed	15	3 (20)†
		Non-inflamed	79	5 (6.3)
Normal liver	20	Non-inflamed	172	5 (2.9)

CVH, chronic viral hepatitis; EBO, extrahepatic biliary obstruction; NASH, non-alcoholic steatohepatitis; p62, p62/sequestosome-1; PBC, primary biliary cirrhosis, SBD, small bile duct.

*$P < 0.01$ vs PBC, non-inflamed and other groups.

†$P < 0.01$ vs normal livers.

‡$P < 0.01$ vs non-inflamed in a same group.

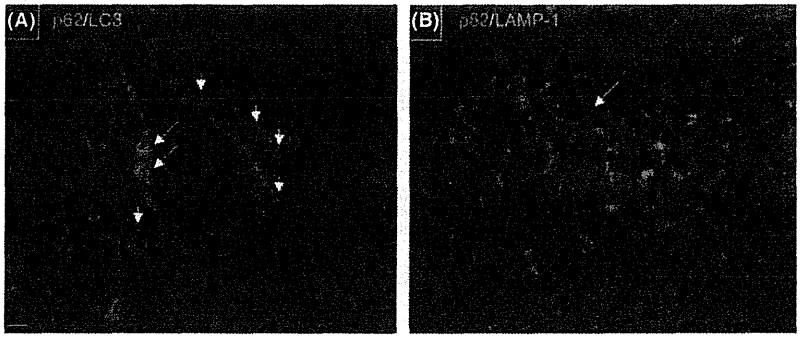

Fig. 2. Co-expression of p62 with LC3 and lysosome-associated membrane protein-1 (LAMP-1) in the inflamed small bile ducts in primary biliary cirrhosis (PBC). (A) The p62-positive aggregates (shown in red) are seen mainly in the supranuclear region in the inflamed small bile ducts in PBC. Whereas, the expression of LC3 (shown in green) is detected in the intracytoplasmic vesicles and some of them are located also in the basal region (short arrows). The colocalization of p62 and LC3 shown in yellow colour is only focal (arrows). Immunofluorescent staining for p62 (shown in red) and LC3 (shown in green). Original magnification, x400. (B) p62-positive aggregates (shown in red) and LAMP1-positive vesicles (shown in green) are detected in the inflamed small bile ducts (arrow). There are few yellow-coloured dots indicating colocalization of p62 and LAMP-1. Immunofluorescent staining for p62 (shown in red) and LAMP-1 (shown in green). Original magnification, x400.

compared with control (0.42 ± 0.3) ($P < 0.01$) (Fig. 7B). The starvation-induced autophagy was significantly inhibited by a treatment with p62 *si*RNA (1.25 ± 1.35), compared with BECs treated with control *si*RNA ($P < 0.01$) (Fig. 7B). Percentage of cells positive for SA-β-gal was significantly increased in cells treated with Etoposide (SA-β-gal labelling index, 18.8 ± 9.04) and serum deprivation (20.9 ± 8.95), when compared with control (1.68 ± 1.78) (Fig. 7C). This result was consistent with our previous reports (11). Significant increase of apoptosis was not induced by treatments with Etoposide (100 μM) and serum deprivation for 4 days (data not shown). The stress-induced cellular senescence was significantly inhibited by a treatment with p62 *si*RNA (Etop, 6.91 ± 5.42; Dep, 3.24 ± 4.25), compared with BECs treated with control *si*RNA ($P < 0.01$) (Fig. 7C).

Discussion

The data obtained in this study are summarized as follows: (i) the p62-positive aggregate was characteristically seen in the inflamed damaged small bile ducts in PBC. (ii) The p62-positive aggregate was co-expressed with LC3 and LAMP-1 in the inflamed and damaged small bile ducts, but the intracytoplamic localization of p62 was different from these proteins, suggesting that p62-positive aggregates may reflect dysfunctional autophagy in primary biliary cirrhosis (PBC). (iii) The accumulation of autolysosomes was ultrastructurally observed in biliary epithelial cells (BECs) in the damaged bile ducts in PBC. (iv) The accumulation of p62 was co-expressed with either of senescent markers, $p16^{INK4a}$ and $p21^{WAF1/Cip1}$ in the inflamed damaged small bile ducts in PBC. (v) Various stress upregulated the expression of p62 in cultured

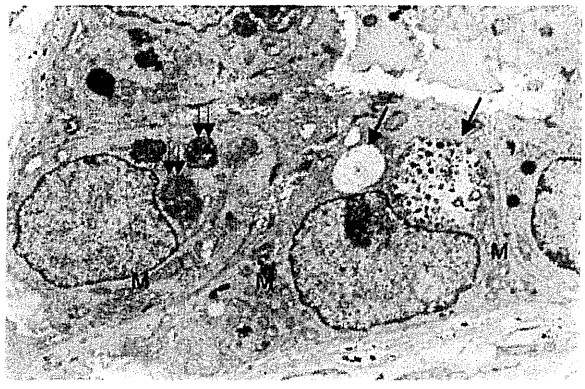

Fig. 3. Accumulation of autolysosomes in the damaged bile duct in primary biliary cirrhosis, stage 1. Several autolysosomes at different stages were observed in biliary epithelial cells. A part of autolysosomes contained degenerative organelle-like structures and myelin-like lamellae (arrows). Autolysosomes with osmiophilic material were also seen (double arrows). These accumulated autolysosomes may be a result of lysosomal dysfunction. Mitochondrial (M) damage is also seen in the form of swelling, disorganization of the cristae. x8000.

BECs, and a treatment with bafilomycin A, a lysosomal inhibitor, further increased p62-positive aggregate. (vi) The knockdown of p62 inhibited significantly autophagy and the stress-induced cellular senescence in cultured BECs.

The present study firstly disclosed that the accumulation of p62-positive aggregates was characteristically seen in the inflamed small bile ducts in PBC. As p62 is a marker of autophagic flux (10,12,28–31,35–37), the increased expression of p62 in the damaged small bile ducts in PBC is consistent with the increased expression of the autophagy marker LC3 in our previous report (11). Although the accumulation of p62 has been reported in hepatocytes in alcoholic hepatitis and hepatocellular carcinoma (32–34), there is no study reporting the involvement of p62 in BECs in biliary diseases, so far. Double immunostaining demonstrated that p62 and LC3 were co-expressed in the same inflamed bile ducts in PBC, but the localization was different. Similarly, p62 and LAMP-1 showed different intracytoplasmic distribution. These findings suggest that p62 may form aggregates outside autophagosome and autophagolysosome.

The accumulation of p62-positive aggregates may reflect dysfunctional autophagy in the inflamed and damaged bile ducts in PBC. The accumulation of p62 in hepatocytes is seen in the animal model of autophagy-deficiency such as Atg5-deficient mouse (10). Cytoplasmic proteinous aggregates including ubiquitinated proteins and p62 were identified as the common morphological hallmark of impaired autophagy in post-mitotic cells (10,35,37,50). Monick *et al.* demonstrated that chronic inhalation of cigarette smoke causes a profound defect in autophagy/lysosomal function showing the accumulation of p62 in human alveolar macrophages (37). Nogalska, *et al.* have reported the impaired autophagy in sporadic inclusion-body myositis with the accumulation of p62 and possible involvement of endoplasmic reticulum stress (50). Taken together, it is plausible that the accumulation of p62 may reflect a decrease of autophagic flux and a dysfunctional autophagy in the inflamed small bile duct (SBD) in PBC.

Electron microscopic analysis disclosed the accumulation of autolysosomes in BECs in the damaged bile ducts in PBC. These accumulated autolysosomes may be a result of lysosomal dysfunction. The accumulation of cytophagosomes and lysosomes containing myelin-like structures has been noted in the small bile ducts in PBC, early stage (41,51). The cytophagosomes included autophagosomes and autolysosomes in these reports (41,51). Therefore, the lysosomal function rather than the early induction of autophagy may be impaired in PBC and the autophagy may be suppressed at the autolysosomal

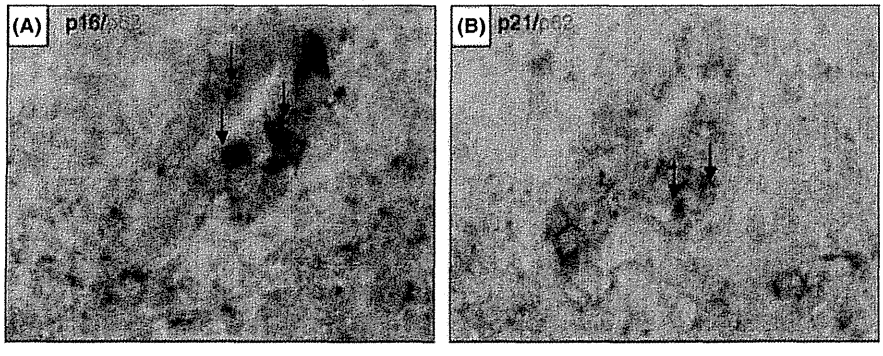

Fig. 4. Co-expression of p62 with senescent markers $p16^{INK4a}$ and $p21^{WAF1/Cip1}$ in the inflamed and damaged small bile ducts in PBC. (A) Nuclear and cytoplasmic expression of senescent marker $p16^{INK4a}$ (shown in blue) was seen in a part of biliary epithelial cells with cytoplasmic p62-positive aggregates (shown in brown) in the inflamed and damaged bile ducts in PBC. (B) Nuclear expression of senescent marker $p21^{WAF1/Cip1}$ (shown in blue) was seen in a part of biliary epithelial cells (arrow). The cytoplasmic p62-positive aggregates (shown in brown) was also seen in the same damaged bile ducts, but it was not colocalized with $p21^{WAF1/Cip1}$ in the same biliary epithelial cells in PBC. PBC, stage 2. Double immunostaining for p62 (shown in brown) and $p16^{INK4a}$ or $p21^{WAF1/Cip1}$ (shown in blue). Original magnification, x400.

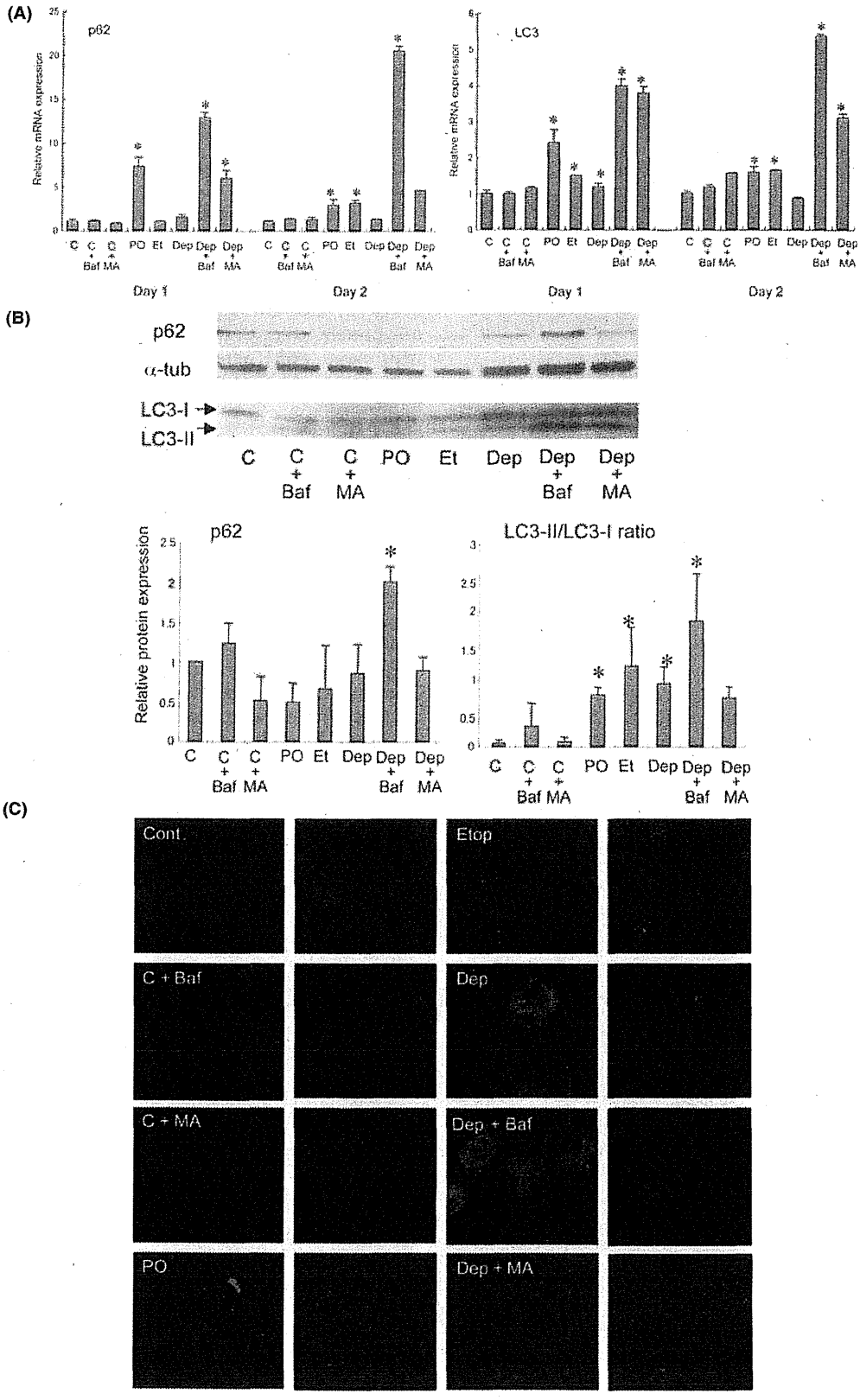

Fig. 5. Increased expression of p62 and LC3 mRNA in biliary epithelial cells induced by treatments with H_2O_2, Etoposide, or serum deprivation. (A) The expression of mRNA in biliary epithelial cells treated with H_2O_2 (PO, 100 μM), Etoposide (Et, 100 μM), or serum deprivation (Dep) with or without Bafilomycin A1 (Baf, 5nM) or 3-methyladenine (MA, 5 mM) was quantified with real-time PCR and normalized as a ratio using β-actin as the housekeeping gene. Data are expressed as the means ± SD. $^*P < 0.01$ compared to the control, n = 6 for each group. (B) The protein level expression of p62 and LC3 assessed by Immunoblot analysis. The protein level of p62 was upregulated by a treatment with Etoposide (Et, 100 μM), serum deprivation (Dep) and serum deprivation with Bafilomycin A1 (Baf, 5 nM). LC3-II/LC3-I ratio, which indicates the level of autophagy, was upregulated by the treatment hydrogen peroxide (PO), Etoposide (Et) and serum deprivation (Dep) with and without Baf. α-tub, α-tubulin; Cont, control. Data are expressed as the means ± SD. $^*P < 0.05$ compared to the control, n = 3 for each group. (C) Immunofluorescent staining for p62 (left column; shown in green) in biliary epithelial cells treated with H_2O_2 (PO, 100 μM), Etoposide (Etop, 100 μM), or serum deprivation (Dep) with or without 3-methyladenine (MA, 5 mM) or Bafilomycin A1 (Baf, 5 nM) for 1 day and no treatment (Cont). Right column, 4′ and 6-diamidino-2-phenylindole (DAPI) nuclear counterstain. The expression of p62 was absent in control (no treatment), whereas p62-positive dots were increased in the cytoplasm of biliary epithelial cells treated by H_2O_2, Etoposide and serum deprivation. The upregulated expression of p62 by serum deprivation was inhibited by a treatment with 3-methyladenine (MA, 5 mM), whereas p62-positive dots induced by serum deprivation were more increased by a treatment with Bafilomycin A1 (Baf, 5nM).

level in the small bile ducts in PBC. The present *in vitro* study also supports this hypothesis. Various stresses induced the accumulation of p62 in cultured BECs and showed similar features to the BECs in PBC. In particular, a treatment with bafilomycin A, which inhibits a fusion of autophagosome and lysosome, further upregulated the accumulation of p62 in BECs treated with serum deprivation. The accumulation of p62 may be induced by similar dysfunctional autophagy in the inflamed and damaged bile ducts in PBC.

Recent studies disclosed that the accumulation of p62 may cause further cell injuries (10,12). For example, Komatsu *et al.* reported that the high level of p62 associated with the suppression of autophagy result in activation of nuclear factor – like 2 (Nrf2) followed by upregulation of detoxifying enzymes and severe liver injury (10). Mathew *et al.* reported that the accumulation of p62 was caused by defective autophagy, induced the elevated reactive oxygen species, activated the DNA damage response and altered signal transduction pathways (12). In a previous report, we have reported the increased expression of oxidative stress markers in the inflamed and damaged bile ducts in PBC (27). This upregulation of oxidative stress markers may be associated with the accumulation of p62 in the bile duct lesions in PBC. Furthermore, the accumulation of p62 in BECs may be related to the altered signalling pathways in the bile duct lesions in PBC.

The present study disclosed that p62 in BECs is closely colocalized with cellular senescence in the inflamed and damaged bile ducts in PBC. This finding is consistent with our previous studies (11) and biliary epithelial senescence in the pathogenesis of bile duct lesions in PBC (24–26). The $p21^{WAF1/Cip1}$ is involved in the induction of senescence, whereas $p16^{INK4a}$ is involved in maintenance of senescence, reportedly (48,49). The co-expression of p62 and $p16^{INK4a}$ was more frequently observed, whereas the co-expression of p62 and $p21^{WAF1/Cip1}$ was rare in the damaged bile ducts in PBC in the present study. The closer co-expression of p62 and $p16^{INK4a}$ may indicate that the accumulation of p62 may be more closely associated with the later stage of cellular senescence. Furthermore, the present study disclosed for the first time that p62 may be involved in the process of cellular senescence in cultured BECs. Interestingly, the knockdown of p62 inhibited the stress-induced cellular senescence as well as autophagy in cultured BECs in the present study.

Autophagy is involved in the process of senescence and the inhibition of autophagy delays the senescence phenotype, including senescence-associated secretion (3,11). On the other hand, the activation of autophagy is thought to have a survival effect, since experimental conditions that extend lifespan in various species, such as dietary restriction and negative modulation of the insulin signalling and TOR pathways (52). Autophagy may be a Janus-face process: the activation of autophagy has a survival effect in a mild and long-term process such as ageing (12,35,52), whereas the deregulated autophagy contributes to senescence establishment in acute and more intense cytotoxic stress (3,11). Recently, Narita, *et al.* reported that spatial coupling of mTOR and autophagy augments secretory phenotypes during RAS-induced senescence (53). Although we did not examine the distribution of mTOR in this study, this system may be involved in biliary epithelial autophagy and senescence in PBC and needs to be addressed. Taken together, the accumulation of p62 caused by cellular stress and dysfunctional autophagy may play a role in the process of biliary epithelial senescence in PBC.

In conclusion, the accumulation of p62-positive aggregates is specifically increased in the damaged bile ducts in PBC and various stress increased the expression of p62 and LC3 and the inhibition of autophagosome-lysosomal fusion enhanced the accumulation of p62. The knockdown of p62 inhibited stress-induced cellular senescence and autophagy. The accumulation of p62 may reflect dysfunctional autophagy, probably at the autolysosomal level, followed by cellular senescence and may be involved in the pathogenesis of bile duct lesions in PBC.

Acknowledgement

This study was supported in part by a Grant-in Aid for Scientific Research (C) from the Ministry of Education, Culture, Sports and Science and Technology of Japan (21590366).

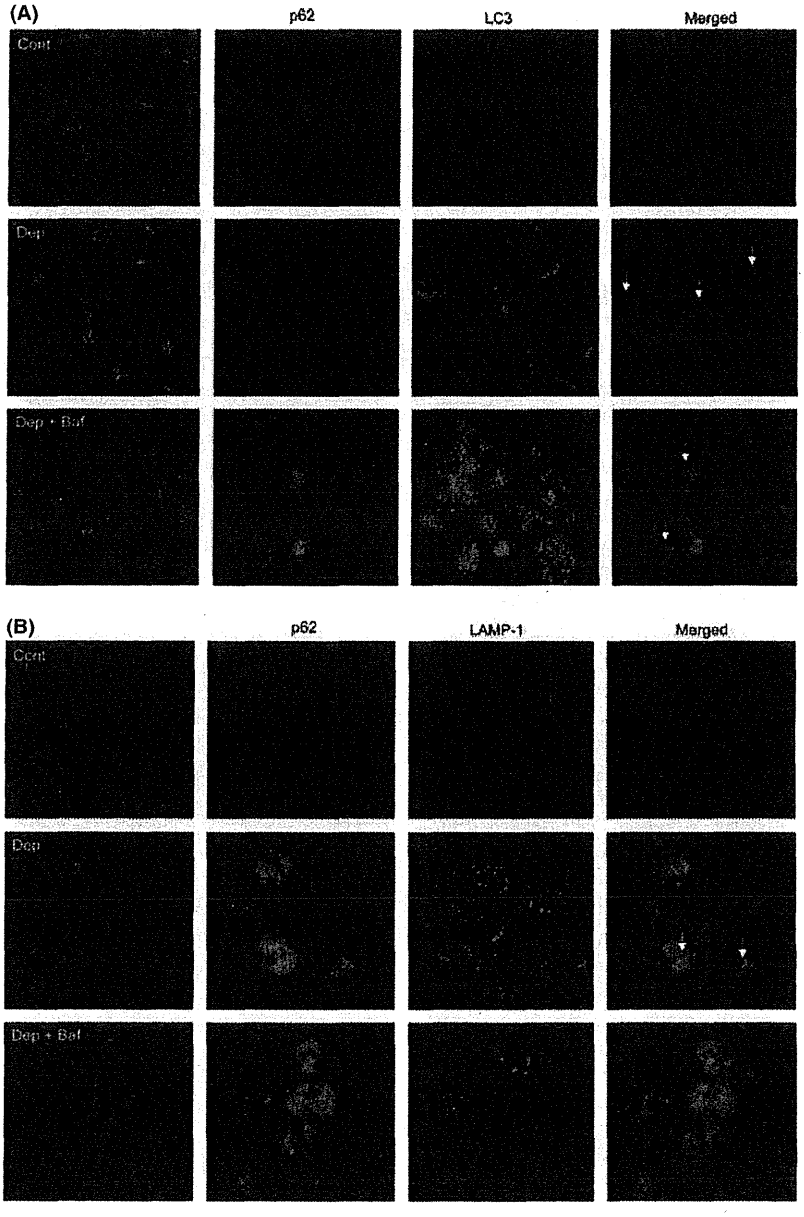

Fig. 6. Co-expression of p62 with LC3 and LAMP-1 in biliary epithelial cells induced by treatments with serum deprivation with and without Bafilomycin A1. (A) Immunofluorescent staining for p62 (shown in red) and LC3 (shown in green). The expression of p62 and LC3 was absent in control (no treatment). Whereas, the cytoplasmic p62-positive dots and LC3-positive dots were increased, and a part of them was colocalized (arrows) by serum deprivation (Dep, 1day). The cytoplasmic p62-positive dots and LC3-positive dots induced by serum deprivation were more increased by a treatment with Bafilomycin A1 (Baf, 5 nM), and there were several p62-positive aggregates in the cytoplasm (arrows). Original magnification, x400. (B) Immunofluorescent staining for p62 (shown in red) and LAMP-1 (shown in green). The expression of p62 and LC3 was absent in control. Whereas, the cytoplasmic p62-positive dots and LAMP-1-positive dots were increased, and a part of them was colocalized (arrows) by serum deprivation (Dep, 1day). The cytoplasmic p62-positive dots induced by serum deprivation were more increased, whereas LAMP-1-positive dots were rather decreased by a treatment with Bafilomycin A1(Baf, 5nM). There were few yellow dots indicating colocalization of p62 and LAMP-1 in the cytoplasm of the biliary epithelial cells. Original magnification, x400.

Author contributions

Motoko Sasaki conceived and carried out experiments and analysed data. Masami Miyakoshi carried out experiments. Yasunori Sato and Yasuni Nakanuma contributed to analyse data. All authors were involved in writing the article and had final approval of the submitted and published versions.